MONTE CARLO CALCULATIONS OF MICROSCOPIC DOSE ENHANCEMENT FOR GOLD NANOPARTICLE-AIDED RADIATION THERAPY

A Thesis
Presented to
The Academic Faculty

by

Bernard Jones

In Partial Fulfillment
of the Requirements for the Degree
Masters of Science in Medical Physics in the
School of George W. Woodruff School of Mechanical Engineering

Georgia Institute of Technology
August 2009

MONTE CARLO CALCULATIONS OF MICROSCOPIC DOSE ENHANCEMENT FOR GOLD NANOPARTICLE-AIDED RADIATION THERAPY

Approved by:

Dr. Sang Hyun Cho, Advisor
School of Mechanical Engineering
Georgia Institute of Technology

Dr. Chris Wang
School of Mechanical Engineering
Georgia Institute of Technology

Dr. Eric Elder
Department of Radiation Oncology
Emory School of Medicine

Date Approved: June 22nd, 2009

ACKNOWLEDGEMENTS

I would like to thank Dr. Sang Cho for his ideas and support during my research work. I would also like to thank the other current and former members of our research group who assisted in this work: Arsalan Siddiqi, Dr. SK Cheong, Fang Liu, and Nivedh Manohar. I am also grateful for the assistance of my thesis committee members Dr. Eric Elder and Dr. Chris Wang. Finally, I would like to thank Dr. Sunil Krishnan of the MD Anderson Cancer Center for providing us with the gold SEM images, and Dr. Vladimir Semenenko of the Medical College of Wisconsin for making the NOREC code available.

TABLE OF CONTENTS

LIST OF TABLES

LIST OF FIGURES

SUMMARY

Gold Nanoparticle-Aided Radiation Therapy (GNRT) is a new paradigm in radiation therapy which seeks to make a tumor more susceptible to radiation damage by modifying its photon interaction properties with an infusion of a high-atomic-number substance. The purpose of this study was to quantify the energy deposition due to secondary electrons from gold nanoparticles on a micrometer scale and to calculate the corresponding microscopic dose enhancement factor during GNRT. The Monte Carlo code EGSnrc was modified to obtain the spectra of secondary electrons from atoms of gold and molecules of water under photon irradiation of a tumor infused with 0.7 weight percent gold. Six different photon sources were used: ^{125}I, ^{103}Pd, ^{169}Yb, ^{192}Ir, 50kVp, and 6MV x-rays. Treating the scored electron spectra as point sources within an infinite medium of water, the event-by-event Monte Carlo code NOREC was used to quantify the radial dose distribution, giving rise to gold and water electron dose point kernels. These kernels were applied to a scanning electron microscope image of a gold nanoparticle distribution in tissue. The dose at each point was then calculated, enabling the determination of the microscopic dose enhancement at each point.

For the lower energy sources ^{125}I, ^{103}Pd, ^{169}Yb, and 50 kVp, the secondary electron fluence was increased by as much as two orders of magnitude, leading to a one-to-two order of magnitude increase in the electron dose point kernel over radial distances up to 50 μm. The dose was enhanced by 100% within 5 μm of the nanoparticles, and by 5% as far away as 30 μm. This study demonstrates a remarkable microscopic dose enhancement due to gold nanoparticles and low energy photon sources. Given that the

dose enhancement exceeds 100% within very short distances from the nanoparticles, the maximum radiobiological benefit may be derived from active targeting strategies that concentrate nanoparticles in close proximity to the cancer cell and/or its nucleus.

CHAPTER 1

INTRODUCTION

Most advances in radiation therapy have been made by modifying the properties of the radiation used to treat the cancer. However, by adjusting the photon interaction probabilities of tumor, it is possible, in principle, to increase or decrease the dose absorbed within the tumor. It is well known that photons have a greater probability of interaction with atoms of a higher atomic number (Z), and so by infusing the tumor with a high Z substance during traditional photon-based therapy, a greater fraction of the incident photon energy can be imparted to the tumor without escalating the damage to the surrounding healthy tissue.

Nanoparticles of sufficiently small size can penetrate the tumor interstitium via the "leaky" vasculature of tumors (Dvorak *et al* 1988), taking advantage of a phenomenon known as "enhanced permeability and retention (EPR)" (Maeda 2003). Through this phenomenon, two targeting scenarios can be envisioned: passive targeting and active targeting. In passive targeting, nanoparticles of 1-100 nm size leak into the tumor interstitium from blood vessels feeding the tumor because they are smaller than the typical 400 nm cutoff size of the pores in the tumor vasculature (Unezaki *et al* 1996). Under an active targeting scenario, nanoparticles are conjugated with antibodies or peptides directed against tumor markers such as epidermal growth factor receptor (EGFR), human epidermal growth factor receptor-2 (HER2), and angiogenesis markers such as vascular endothelial growth factor receptor (VEGFR). For either of these approaches, gold nanoparticles are singled out among various metal nanoparticles, as

they are chemically inert, and as a result, are biologically non-reactive and molecularly stable.

In the past, researchers have examined several methods of radiosensitization/dose enhancement using high-Z materials, focusing mainly on iodine or other similar computed tomography (CT) contrast agents during kilo-voltage irradiation (Mello *et al* 1983, Dawson *et al* 1987, Iwamoto *et al* 1987, Rose *et al* 1994, Mesa *et al* 1999, Robar *et al* 2002, Verhaegen *et al* 2005, Robar 2006). One would imagine that an approach utilizing gold nanoparticles has the potential to be more effective due to both the higher Z of gold and the greater tumor specificity of properly sized nanoparticles. An animal study (Hainfeld *et al* 2004) demonstated the effectiveness of the EPR process, finding that mice irradiated after injection of gold nanoparticles demonstrated remarkable tumor regression and long-term survival compared to mice irradiated without gold present. The increase in dose deposition was quantified by a subsequent Monte Carlo study, and showed that the macroscopic dose enhancement depended on both the gold concentration and photon beam quality, ranging from a few percent for megavoltage beams to several hundred percent for diagnostic x-rays (Cho 2005). These results were also confirmed by a theoretical study based on the energy-dependent absorption coefficients of different materials (Roeske *et al* 2007).

It has been shown that gold enhances dose to a tumor through an increase in the amount of photoelectric absorption, which can lead to an increase of up to two orders of magnitude in the number of photoelectrons produced (Cho *et al* 2009). Therefore, it is important to carefully choose the photon source spectrum to maximize the fraction of photoelectric absorptions. Brachytherapy is well-suited to this approach, as typical

radionuclide seed sources such as ^{125}I, ^{103}Pd, and ^{192}Ir emit photons primarily in the keV range. Photoelectric absorption can be enhanced further by selecting a source with a preponderance of photons just above the absorption edges of gold. For example, an HDR ^{169}Yb source has an intensity-weighted average energy of about 93 keV (Medich *et al* 2006), just exceeding the gold K-edge of 80.7 keV.

While it has been shown computationally that gold nanoparticles can increase dose deposition during brachytherapy by over 100% (Cho *et al* 2009), it is not known exactly how a nanoparticle influences the dose on the micrometer scale. Due to the short range of 10-100 keV electrons, it is likely that the dose may be concentrated in the vicinity of the nanoparticles, leading to an even more dramatic increase in dose for nearby tumor cells. This information could be crucial in deciding between passive or active nanoparticle targeting scenarios.

By using the secondary electron spectra of gold and water during gold nanoparticle-aided radiation therapy (GNRT), the goal of this study was to calculate the microscopic dose deposition kernels of gold nanoparticles for six different source photon spectra: ^{125}I, ^{103}Pd, ^{169}Yb, ^{192}Ir, 50 kVp x-rays, and 6 MV x-rays. These spectra are then used to explicitly calculate the microscopic dose enhancement for a given nanoparticle biodistribution, and give great insight into the area of effect of a gold nanoparticle under photon irradiation. Ultimately, the current presentation aims to provide the impetus for further investigation and clinical implementation of GNRT for many types of cancers that can be treated with brachytherapy.

CHAPTER 2

BACKGROUND

2.1 Monte Carlo Method

The Monte Carlo method is a computational tool whereby one may avoid performing stochastic calculations that may be difficult or impossible. It is a way of stochastically computing different quantities based on random simulations of events with knowledge of the probabilities associated therein. The most common example is to calculate the value of π. Imagine a circle inscribed within a square of area 1. As points are chosen randomly within the square, they may be tested as to whether they lie within the circle. As the number of points chosen increases, the ratio of the number that fall within the circle to the total number of points begins to approximate the ratio of the area of the square to the area of the circle, or $\pi/4$. As with most Monte Carlo simulations, the results are governed by Poisson statistics, and thus the error decreases as the square root of the number of simulations performed.

The distribution of sub-atomic particles within a medium can also be determined using the Monte Carlo method, given that one knows enough details about the system in question. Given a source of particles within some system whose geometry is known, the paths, or histories, of those particles can be simulated if one knows the probabilities that govern any interaction that particle could experience. One may then record any data of interest, such as the number of particles crossing a volume or energy spectrum of particles, and as the total number of histories increases these quantities begin to approximate the true value of the system.

For uncharged particles, the number of interactions per history is generally small enough such that it is feasible to simulate every interaction explicitly. For uncharged particles, this is not the case. Monte Carlo codes can be divided into two types: those that simulate every interaction of charged particles and those that average together many particle interactions into a single step. The first type of code is known as a track structure, detailed history, or event-by-event code. Simulating every charged particle interaction is very computationally expensive, and often one may gain this detailed track information at the cost of being able to simulate complex geometry or materials. For instance, the detailed history electron Monte Carlo code NOREC (Semenenko *et al* 2003) is able to perform event-by-event transport of electrons, but only in an infinite medium of liquid water. The second type is known as a condensed history code; it performs a charged particle step that samples energy loss and angle change as though the particle had interacted many times. The size of the step is usually on the order of 1 cm. Most Monte Carlo codes fall under this category, as it is fast and yields accurate results.

2.2 EGSnrc Code System

EGSnrc is a Monte Carlo code which performs coupled transport of photons and electrons. It is distributed under a license owned by the National Research Council of Canada (NRC), and is built upon the EGS4 code developed by the Stanford Linear Accelerator Center (SLAC). The history of EGSnrc can be traced back to the 1970's, when Richard Ford at SLAC generalized existing Stanford codes to be able to run in any medium through the use of preprocessing routines (Bielajew *et al* 1994), and the resulting codes were known as Electron Gamma Shower (EGS) and Preprocessor for EGS (PEGS). As processing power increased, it became clear that it would not be feasible to construct a

self-contained code able to perform all of the scoring and output options necessary, or a geometry package that could handle arbitrarily complex geometries. The EGS code system was stripped of these functions, and it was left to the user to handle the geometry and scoring routines. As of 1994, the EGS community had grown to over 6000 people, contributing to the development of what has been termed EGS user codes. These codes, written in an extended FORTRAN IV language called MORTRAN, were created to perform electron/gamma transport for different geometries or for different scoring requirements. For instance, the codes DOSXYZ and DOSRZ were written to record dose in a Cartesian or cylindrical phantom, respectively, while the code BEAM was written to record the photon output of a clinical linear accelerator.

EGSnrc is capable of performing photon and electron transport for particles ranging from a few keV to several hundred GeV. The code takes into account many physical processes, including Bremsstrahlung production, positron annihilation (in-flight or at rest), Moller (e^-e^-) and Bhabha (e^+e^-) scattering, pair production, bound Compton scattering, coherent scattering, photoelectric effect, and relaxation of exited atoms. It performs electron transport using the condensed history method, using an algorithm that can perform electron steps of any size. The code shifts between single scattering models for short step sizes and multiple scattering models for larger steps, and has the ability to correct for relativistic and spin effects. Additionally, continuous energy loss is applied to charged particles in between discrete interactions (Kawrakow and Rogers 2003). The PEGS4 preprocessing code is able to generate material data for any element up to atomic number 100.

2.3 NOREC Code System

The NOREC code is an event-by-event Monte Carlo code developed by Semenenko, Turner, and Borak in 2003 to address deficiencies in the Oak Ridge electron transport code (OREC). The original aim was to incorporate a better elastic scattering model, but close scrutiny of the code resulted in several other changes, as well as the translation of the code to the C++ language. NOREC calculates event-by-event transport of electrons in liquid water for energies ranging from 1 MeV to 7.4 eV, the threshold for electronic transitions in liquid water. The main improvement from OREC was the addition of differential cross sections from the National Institute of Standards and Techonology (NIST) to calculate elastic scattering of electrons above 1 keV by atoms (Semenenko *et al* 2003).

Transport with NOREC is implemented as a C++ class within a user-generated code. The user is required to provide routines to handle source distributions, geometry, and particle scoring. An element of the NOREC class is initialized with the primary electron location and energy, and subsequent calls to the element return the location and energy of the next collision of the primary electron or its progeny. Event-by-event calculations are performed until the electron falls below 10 eV. In this region, the chance of elastic scatter begins to dwarf that of inelastic scatter, leading to large increases in computing time for a particle with very little energy left to deposit. Based on the results of more detailed studies in this energy region, particles under 10 eV are transported by one additional step and assigned an energy value below the 7.4 eV threshold.

CHAPTER 3

METHODOLOGY

The calculations for this work were performed in three steps. In the first step, the spectra of secondary electrons were calculated using a condensed history Monte Carlo code. In the second step, the dose point kernels of these spectra were calculated with a event-by-event Monte Carlo code. Finally, these point kernels were applied to an image of gold nanoshells in tissue.

3.1 Calculation of Gold and Water Secondary Electron Spectra

The Monte Carlo code EGSnrc (Kawrakow and Rogers 2003) was modified to output the energy and origin of each electron liberated through the photoelectric, Compton, or Auger processes, allowing the calculation of the secondary electron spectra of gold nanoparticles. Six photon source spectra were considered: ^{125}I, ^{103}Pd, ^{169}Yb, ^{192}Ir, 50kVp x-rays, and 6MV x-rays. Except in the case of 6 MV x-rays, the phantom geometry reflected a typical brachytherapy treatment, and was composed of a 3x3x3 cm^3 tumor centered in a 30x30x30 cm^3 water phantom. To mimic a brachytherapy seed source, the source region was a 0.01x0.01x1 cm^3 volume in the center of the tumor. For the 6 MV case, a 4x4 cm^2 field was incident at 100 cm source-to-surface distance (SSD) on the front face of a 30x30x30 cm^3 water phantom. The tumor was a 3x3x3 cm^3 region at a depth of 5-8 cm in the phantom along the beam's central axis. Two simulations were performed: one with the tumor composed of water and 0.7 weight percent (wt %) gold and one with no gold present. By tracking the atom of origin for each electron, the spectra were separated into those of gold and water.

The six photon source spectra were chosen in an attempt to replicate realistic treatment scenarios. For ^{125}I, ^{103}Pd, and ^{169}Yb, measured spectra of physical brachytherapy seeds or sources were used (Ling *et al* 1983, Chen and Nath 2001, Medich *et al* 2006). For ^{192}Ir, the spectrum of a microSelectron HDR source that is included with EGSnrc was used. The 6 MV beam was that of a Varian clinical accelerator (Cho *et al* 2005). The 50 kVp source was intended to represent a miniature x-ray delivery device, and the spectrum used was that of a beam with 1.5 mm Al filter and 17° W target (Birch *et al* 1979). These source spectra are displayed in Table 3.1 and Figures 3.1-2.

Table 3.1: Brachytherapy Source Spectra (and Half-Life)

^{125}I (59.4d)		**^{103}Pd (17.0d)**		**^{169}Yb (32.0d)**		**^{192}Ir (73.8d)**	
Energy (keV)	Relative Intensity	Energy (keV)	Relative Intensity	Energy (keV)	Relative Intensity	Energy (keV)	Relative Intensity
22.1	0.25	20.1	6.41E-01	49.5	0.160	0 - 65	0.040
25.2	0.07	22.7	1.55E-01	50.7	0.283	65 - 70	0.006
27.4	1.00	29.9	3.37E-04	57.6	0.089	70 - 75	0.011
31.4	0.25	39.8	3.84E-03	59.1	0.025	75 - 80	0.001
35.5	0.06	42.5	1.47E-03	63.1	0.133	150 - 200	0.002
		45.1	1.77E-04	93.6	0.008	200 - 205	0.004
		59.5	1.43E-05	109.8	0.053	205 - 210	0.016
		62.5	1.23E-05	118.2	0.006	210 - 280	0.002
		64.5	1.04E-05	130.5	0.034	280 - 285	0.003
		66.8	1.62E-05	177.2	0.067	285 - 290	0.002
		280.4	2.88E-05	198	0.108	290 - 295	0.003
		294.8	2.85E-05	261.1	0.005	295 - 300	0.148
		319.3	3.48E-04	307.7	0.030	300 - 305	0.002
		344.6	3.11E-05			305 - 310	0.158
		357.3	2.16E-04			310 - 315	0.002
		496.9	3.28E-05			315 - 320	0.435
		1115.6	4.00E-05			370 - 375	0.004
						415 - 420	0.004
						465 - 470	0.274
						480 - 485	0.019
						485 - 490	0.003
						585 - 590	0.025
						600 - 605	0.049
						610 - 615	0.031
						880 - 885	0.001

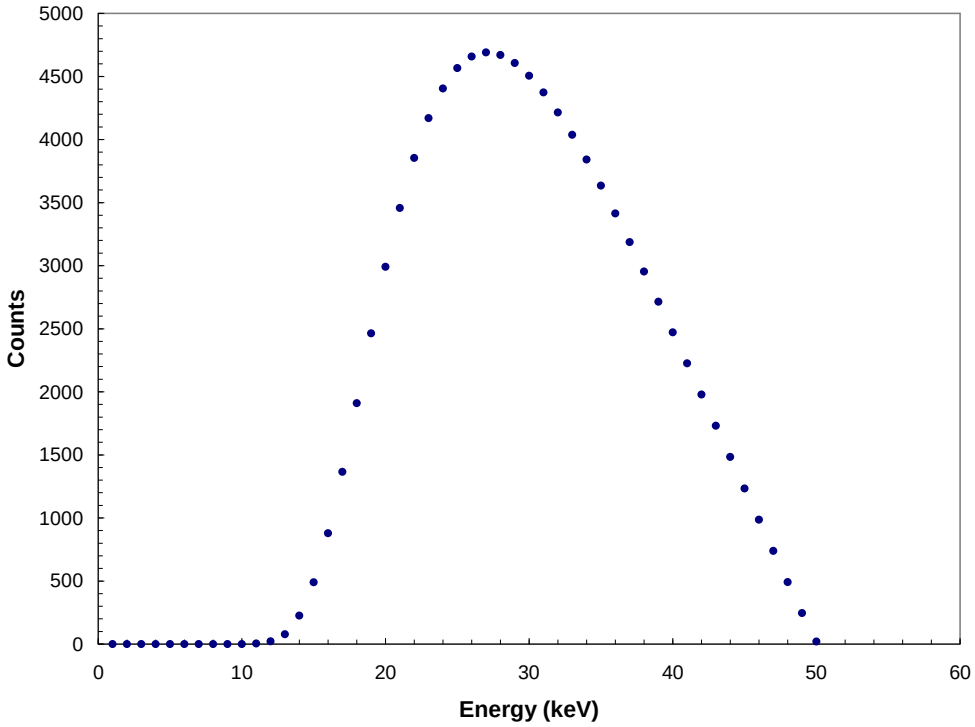

Figure 3.1: 50 kVp X-ray Spectrum

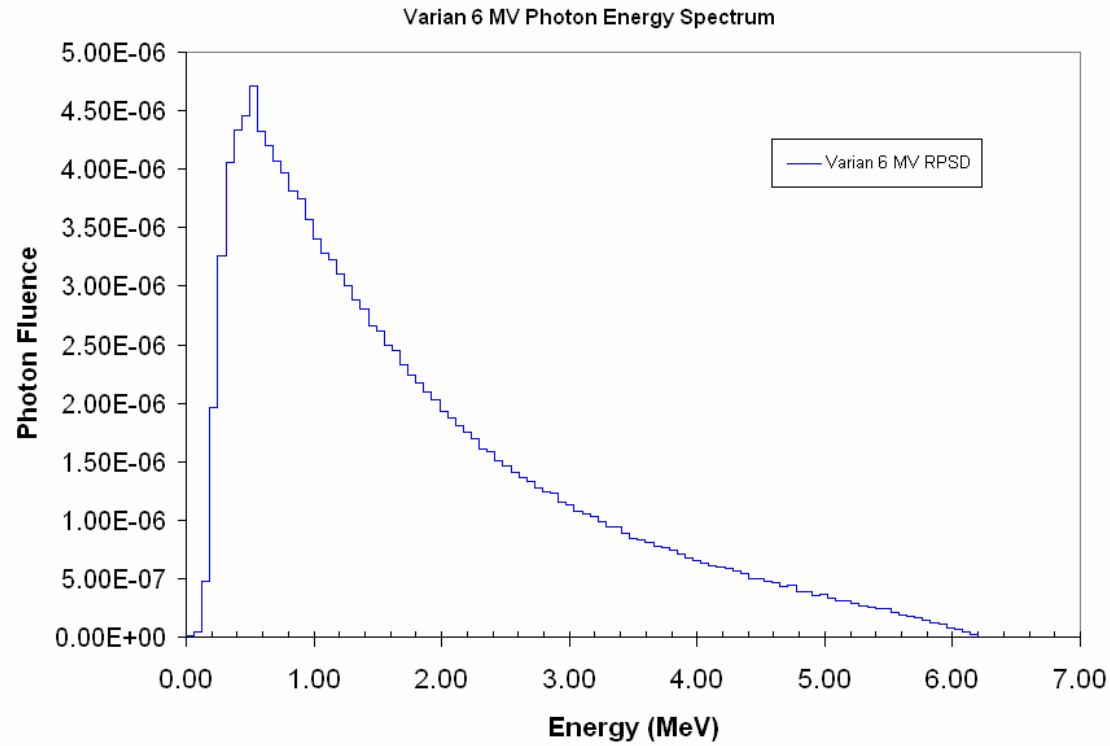

Figure 3.2: Varian 6 MV Photon Spectrum

3.2 Calculation of Secondary Electron Point Dose Kernels

In order to determine the microscopic dose distribution due to secondary electrons, the detailed history electron Monte Carlo code NOREC (Semenenko *et al* 2003) was used. To obtain accurate results, it was important to utilize an event-by-event code rather than a condensed-history code due to the fact that the intended spatial resolution of the dose distribution (< 1 μm) is much smaller than the standard electron step size of codes such as EGSnrc or MCNP. NOREC is implemented as a C++ class which performs event-by-event transport of electrons in water with energy as high as 1 MeV. The effects of this energy limitation on sources with higher energy components such as ^{103}Pd and 6 MV x-ray are addressed during the presentation of the results.

The calculations were performed by treating each spectrum as a point source of electrons in an infinite medium of water. The energy deposition of the electrons was recorded in a set of 0.1-μm-thick concentric spherical shells out to a maximum radial distance of 500 μm. The uncertainty in dose was calculated by tracking the number of deposition events in each shell and calculating the Poisson standard deviation of $N^{-1/2}$. The uncertainty in each significant region (with dose greater than 1% of maximum) in all cases was less than 1%.

3.3 Application of Point Dose Kernels to an Image

To simulate the effects of the nanoparticle dose kernels and calculate the microscopic dose enhancement due to the presence of gold, the kernels applied to a scanning electron microscopy (SEM) image of a gold nanoshell distribution in tissue having a gold concentration of roughly 10 μg Au/g tumor, shown in Figure 3.3. Note that, due to the size of gold nanoshells, there is little penetration from the tumor

vasculature into the interstitium. This image was, however, the best way to test the effect of the gold secondary electrons. Since the nanoshells appear as white pixels in the image, it was first filtered to replace all non-white pixels with black. Then, each pixel in the image was treated as a point source of secondary electrons depositing dose radially around it in the form of the electron dose point kernels calculated previously.

The dose enhancement calculation was performed in two steps under the assumption that the gold nanoshell distribution in three dimensions is similar to that of the two-dimensional image used. First, the equilibrium dose, or the dose with no gold, was calculated using a 5000 by 5000 matrix of pixels. Using the same pixel-to-μm scale as the image, the dose contribution of every pixel in the image was summed for the center pixel. In the second part of the simulation, the dose contribution of each gold pixel in the image was found for every other pixel by adding in the difference of the gold and water 2-D radial energy deposition at that distance. Finally, the energy deposition collected at each point was divided by the equilibrium dose, to yield the factor by which the dose is enhanced at that point by the inclusion of gold nanoshells.

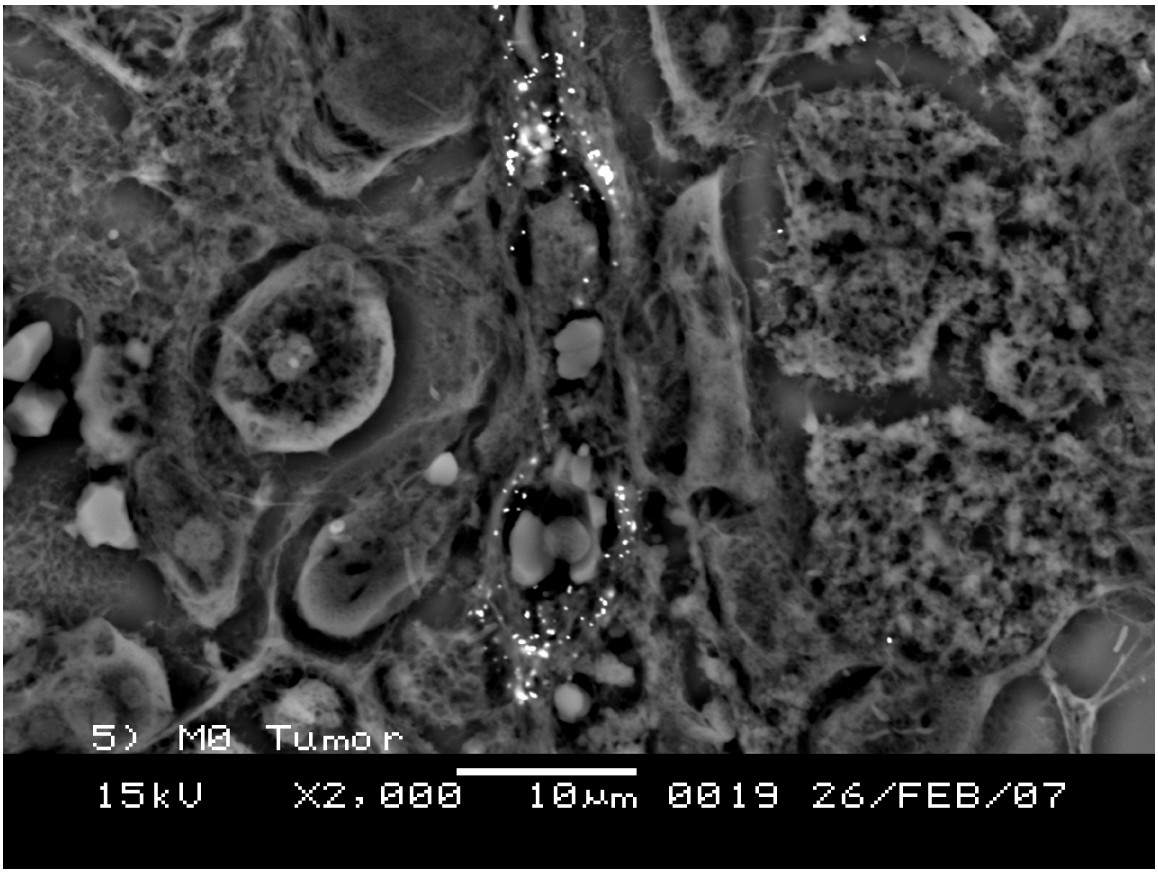

Figure 3.3: SEM Image of Gold Nanoshells in Tissue

CHAPTER 4

RESULTS

4.1 Secondary Electron Spectra

The modifications to the EGSnrc code yielded secondary electron spectra for each of the six photon sources used. A summary of these spectra is shown in Tables 4.1-2, and the full spectra are shown in Appendix A. As expected, the majority of the secondary electrons were produced by the photoelectric and Auger processes, and the majority of the dose deposited can be attributed to photoelectrons.

Table 4.1: Secondary Electrons Produced in Gold per 100 Source Photons

Source	Photoelectric	Compton	Auger	Total
50 kV	29.95	0.05	55.52	85.52
^{125}I	32.89	0.04	60.77	93.71
^{103}Pd	43.81	0.02	80.94	124.77
^{169}Yb	6.77	0.12	12.55	19.43
^{192}Ir	0.77	0.11	1.46	2.34
6 MV	0.08	0.02	0.01	0.11

Table 4.2: Energy of Secondary Electrons (keV) in Gold per Source Photon

Source	Photoelectric	Compton	Auger	Total
50 kV	4.739	0.001	2.018	6.759
^{125}I	5.28	0.00	2.25	7.53
^{103}Pd	4.329	0.000	2.926	7.255
^{169}Yb	2.835	0.018	0.469	3.321
^{192}Ir	0.914	0.102	0.061	1.077
6 MV	0.096	0.110	0.002	0.207

4.2 Electron Point Dose Kernels

In order to compare the point kernel results between different cases, several corrections were necessary. First, the energy deposition per electron at each radial location was divided by the maximum energy deposition to yield the electron dose point kernel. This kernel is shown in Figure 4.1 and is defined as the fraction of the maximum dose deposited at each radial location. The dose point kernel depends strongly on the quality of the secondary electron spectrum, as evidenced by the sharp dose fall-off in the lower energy sources (^{103}Pd, ^{125}I, 50 kVp) as compared to the higher energy sources.

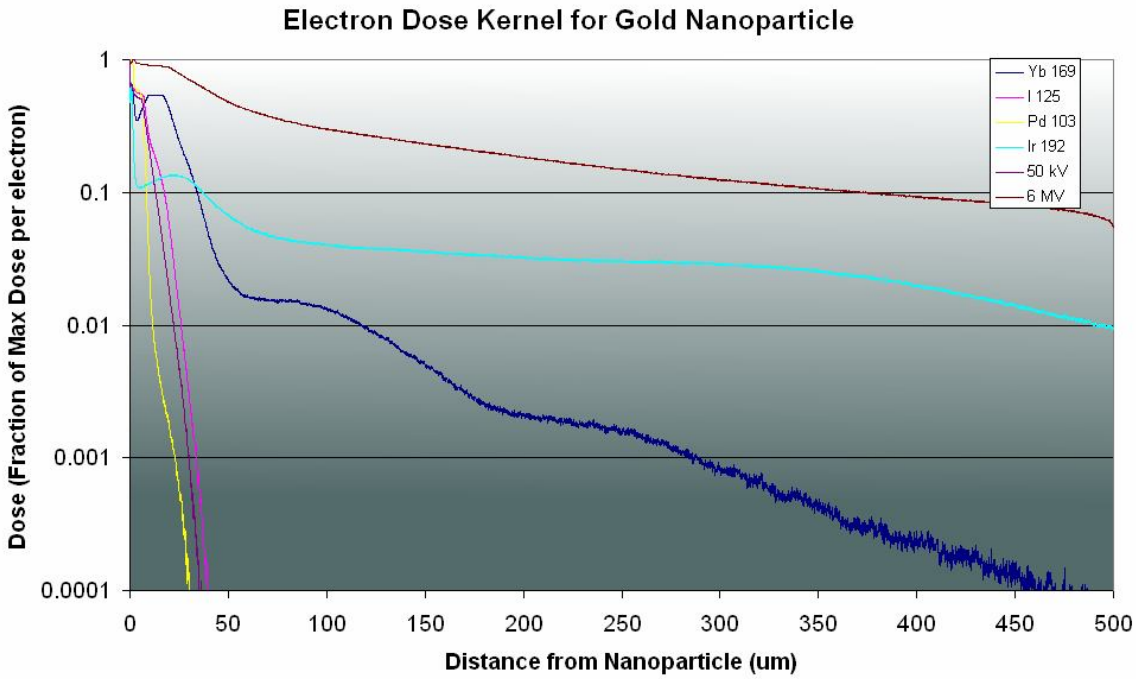

Figure 4.1: Electron Dose Kernel for Secondary Electrons Emitted by Gold

For each source, the dose point kernel gives insight into the range of effect of gold nanoparticles during treatment. For ^{103}Pd, ^{125}I, and 50 kVp, it is apparent that the gold nanoparticles would only significantly affect the region within 30-40 μm. For ^{169}Yb, the dose point kernel is greater than 1% for distances as far as 100 μm, while for ^{192}Ir and 6 MV x-rays the dose kernel extends out beyond the 500 μm range. In the case of the 6

MV x-ray dose kernel, NOREC was unable to simulate those secondary electrons with energy greater than 1 MeV. However, in the microscopic range less than 500 μm, one would not expect to see much difference in energy deposition between a 1 MeV electron and a 6 MeV electron, whose continuously slowing down approximation (CSDA) ranges of 0.44 cm and 3.1 cm both greatly exceed the current problem domain. Thus, the inclusion of electrons greater than 1 MeV would lead to much the same result: a dose kernel with a relatively gentle slope that extends beyond 500 μm.

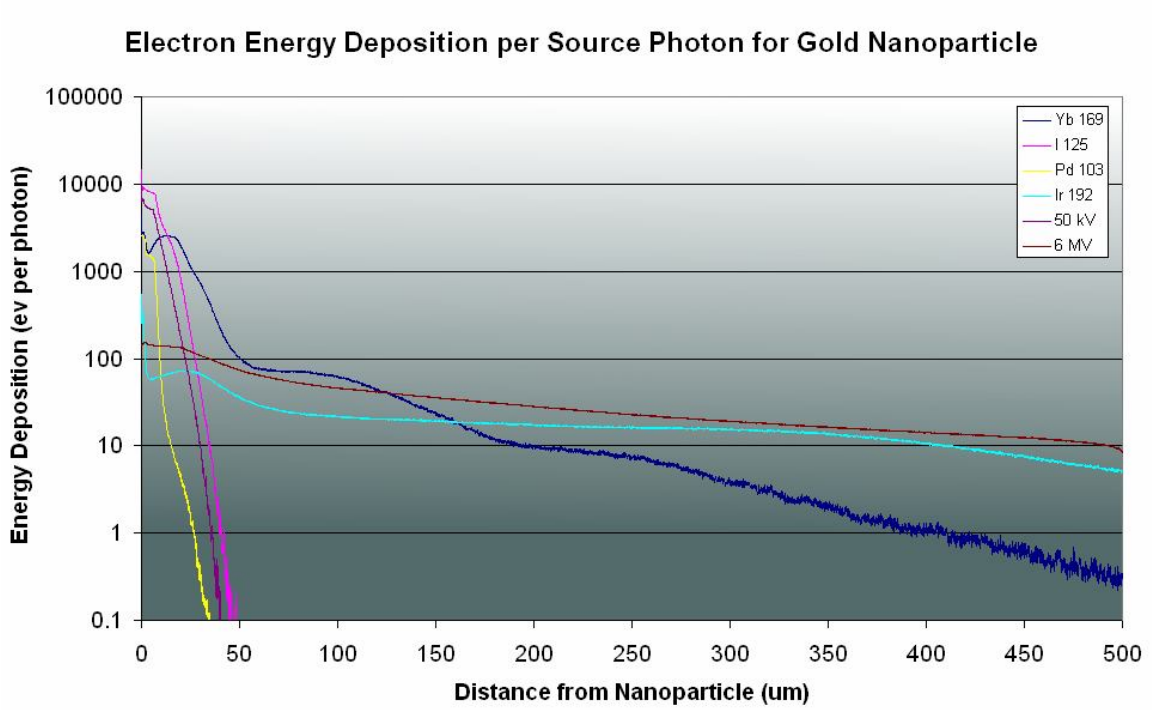

Figure 4.2: Electron Energy Deposition per Source Photon

To calculate the dose enhancement due to the gold nanoparticle, the energy deposition results were converted from energy per secondary electron to energy per incident photon. This accounts for the fact that a photon is much more likely to interact with an atom of gold than a molecule of water. The secondary electron spectra were summed over all energies, yielding the number of electrons emitted per photon for both gold and water. The correction factor was then the ratio of this quantity for gold and

water. Another correction factor was necessary to account for the much higher concentration of water molecules than gold atoms. This correction factor normalized the results to one quanta of gold (or water), and was simply the ratio of the water molecular density to the gold atomic density.

The application of this correction yields the curves for electron energy deposition per source photon, shown in Figure 4.2. One can see the benefit of a lower energy source spectrum, as the increased contribution of photoelectric absorption in gold creates many more secondary electrons per incident photon. ^{125}I, ^{103}Pd, ^{169}Yb, and 50 kVp, all having a strong source component below the K-edge of gold, show a substantial increase in energy deposition below 50 μm. ^{169}Yb especially, with an average energy very close to the K-edge of gold, shows a large amount of electron energy deposition even as far away as 100 μm.

In order to quantify the effect that gold nanoparticles would have during radiation therapy, a comparison was made between the energy deposition per photon of the gold secondary electron spectrum to that of water. The ratio of these two values at a specific radial location yielded the enhancement in dose kernel due to the inclusion of gold nanoparticles within the tumor. Considering only dose originating from a single point of water, this number represents the factor by which that dose would be increased by replacing that point with a gold nanoparticle.

The enhancement in the dose kernel is shown in Figure 4.3 for all sources. These values are only shown out to a radial distance of 100 μm, as the energy deposition beyond that distance is negligible. As expected, the dose kernel increase in the area immediately surrounding the gold nanoparticle is quite large, being at least 100% for all cases, and

over 1000% for all but the 6 MV source. The effects of a lower energy source spectrum are again evident, as the ^{125}I, 50 kVp, and ^{169}Yb spectra show a two order of magnitude dose kernel increase over short distances.

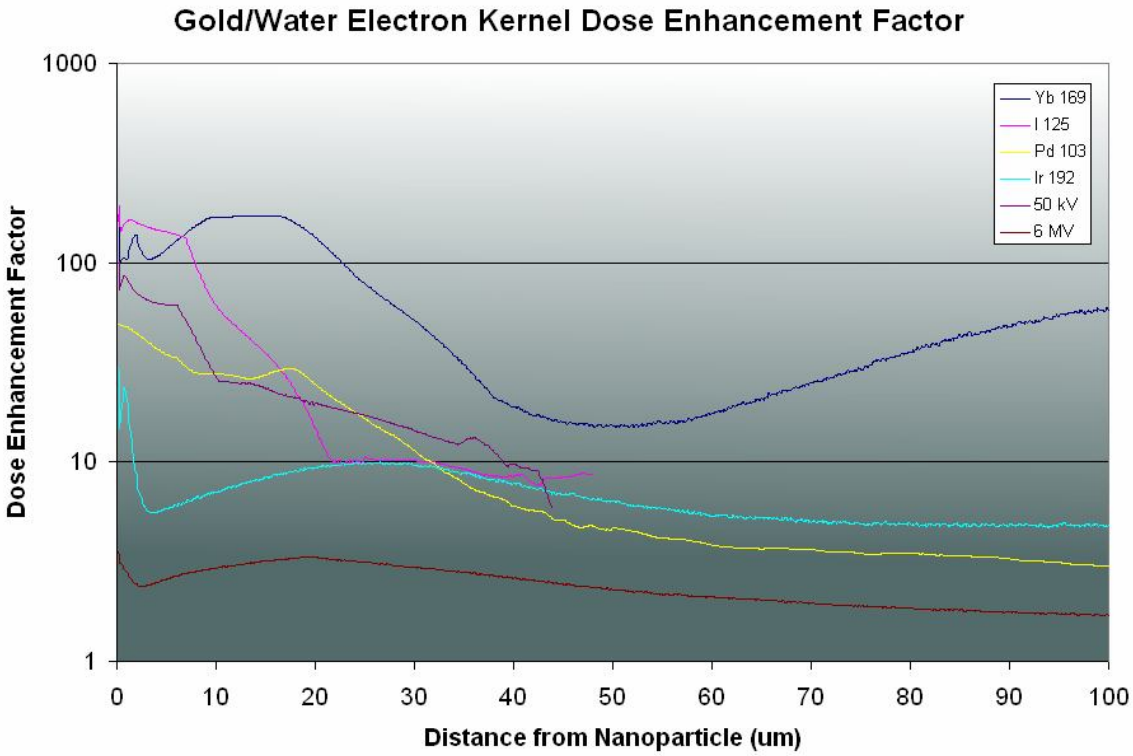

Figure 4.3: Enhancement in Dose Kernel between Gold and Water Secondary Electrons

4.3 Microscopic Dose Enhancement Factor

The microscopic dose enhancement due to gold nanoparticles in the sample image, defined as the ratio of dose deposited at each point between the gold and water cases, is shown in Figures 4.4-7 for all sources apart from ^{192}Ir and 6 MV, for which there was not substantial dose enhancement above 5%. The 50 kVp, ^{125}I, and ^{103}Pd sources, which contained the strongest low-energy component, demonstrated a microscopic dose enhancement factor (mDEF) as high as 5 within the tumor vasculature, corresponding to a dose enhancement of 400%. One can also see that the 5% enhancement line extends 10-15 μm from the nanoparticle clusters. The greatest effect was seen in the ^{169}Yb

source, where the 5% enhancement line extended upwards of 25 μm from the nanoparticle clusters, and the mDEF inside the vasculature exceeded 2. Figure 4.8 shows the extent of the 5% enhancement line for all sources.

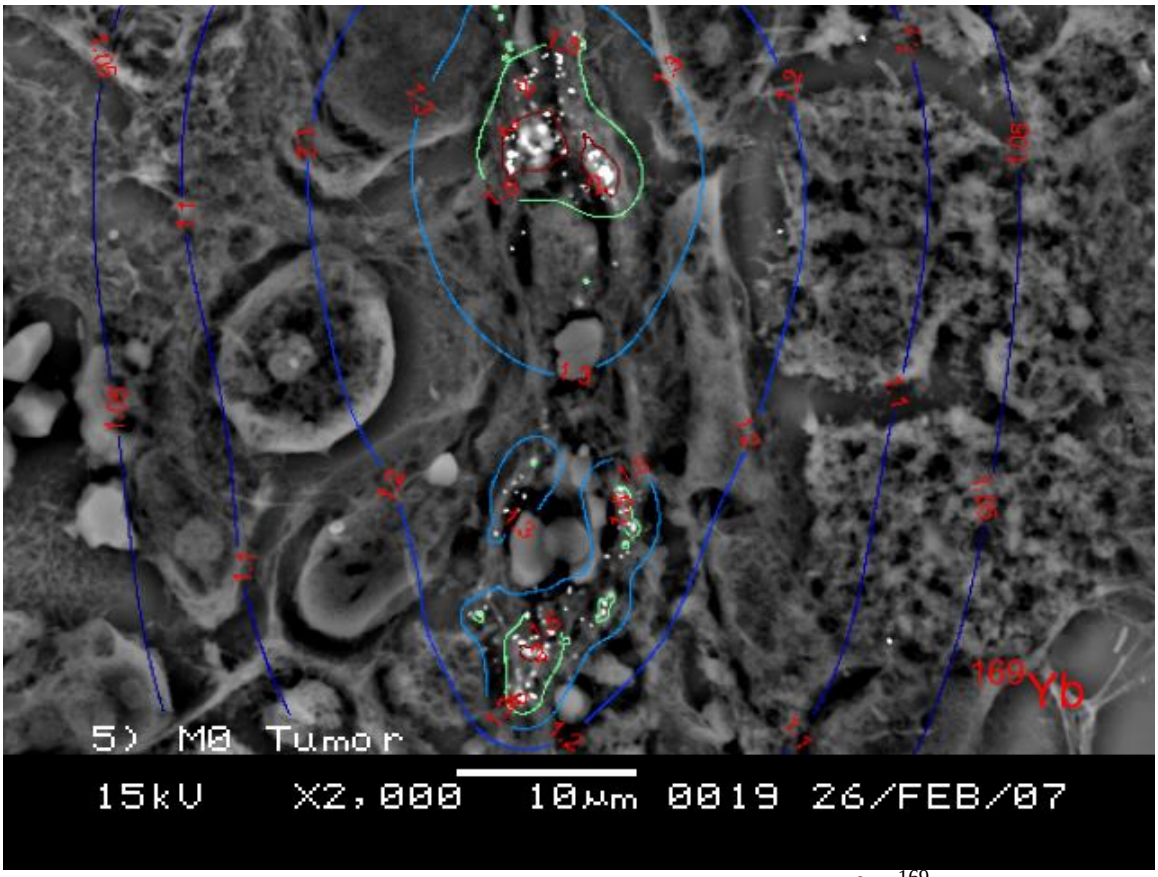

Figure 4.4: Microscopic Dose Enhancement Factor for ^{169}Yb

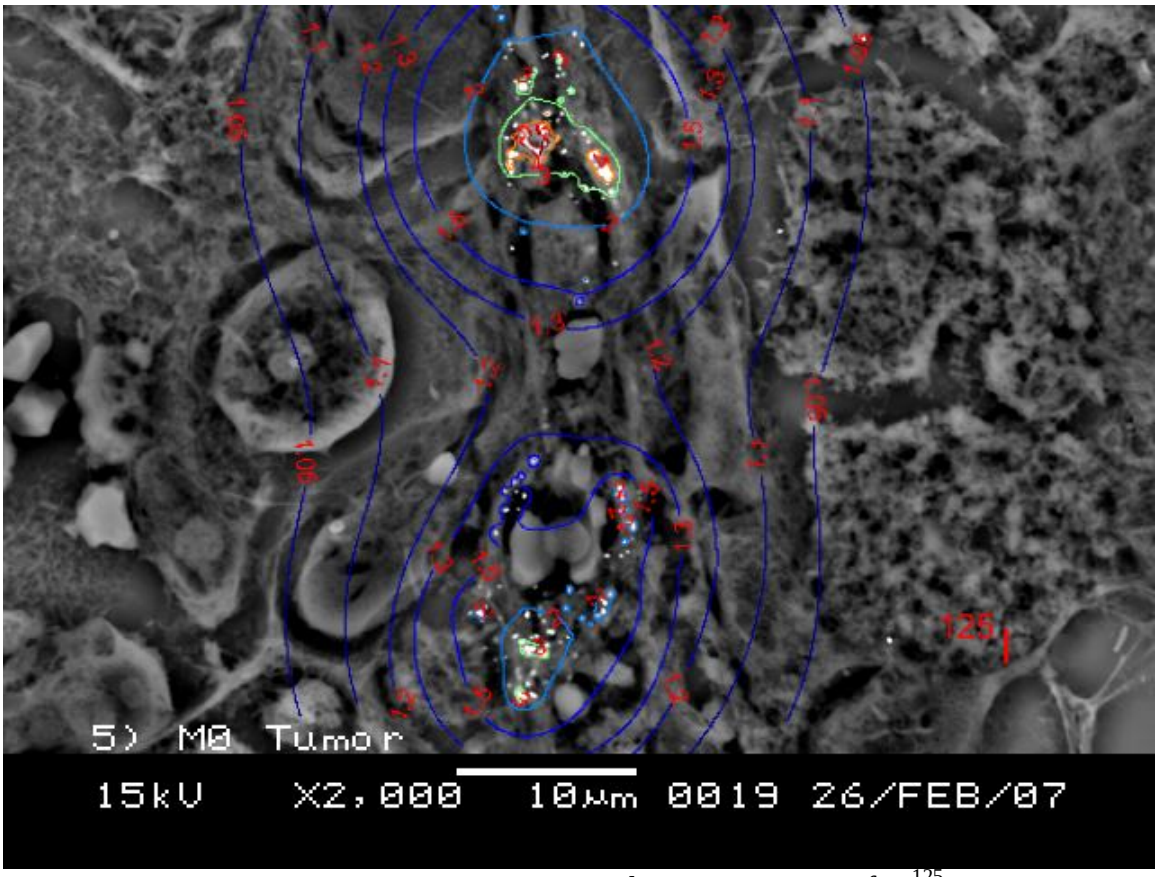

Figure 4.5: Microscopic Dose Enhancement Factor for ^{125}I

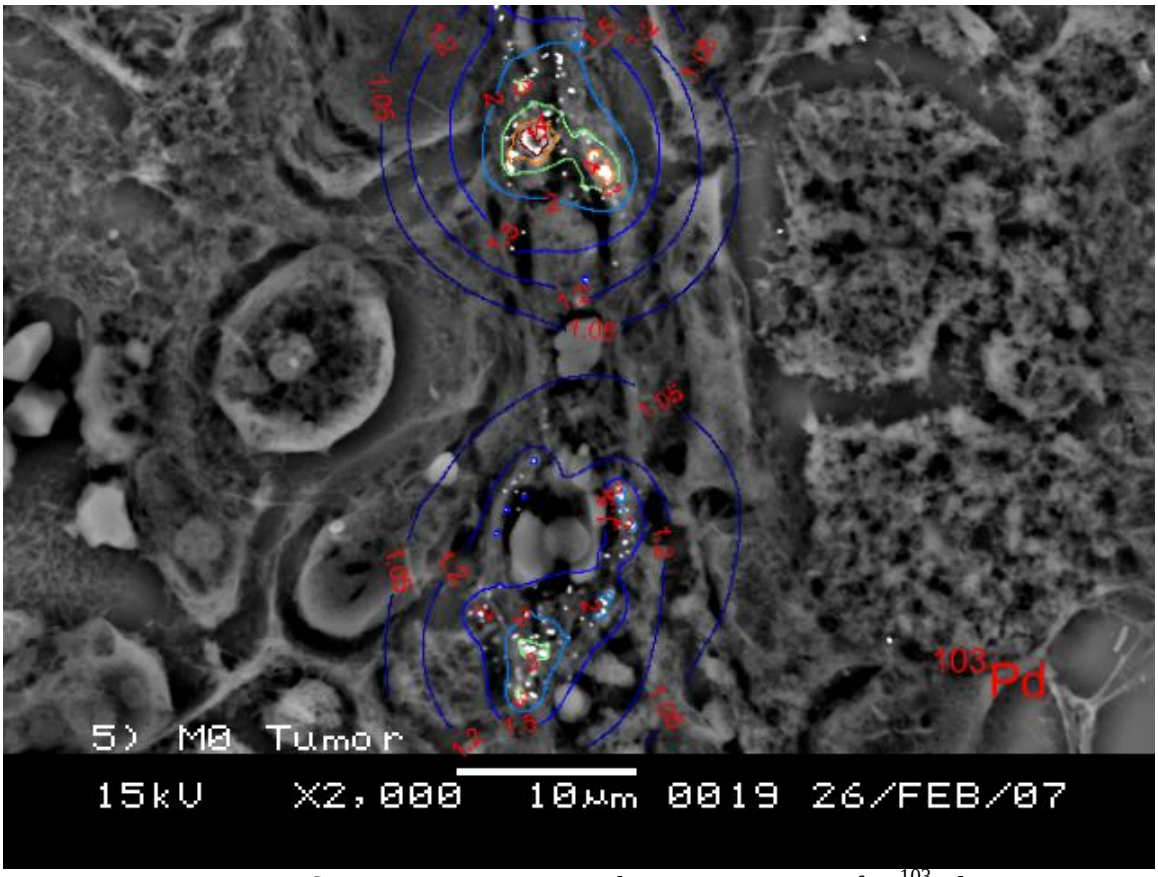

Figure 4.6: Microscopic Dose Enhancement Factor for ^{103}Pd

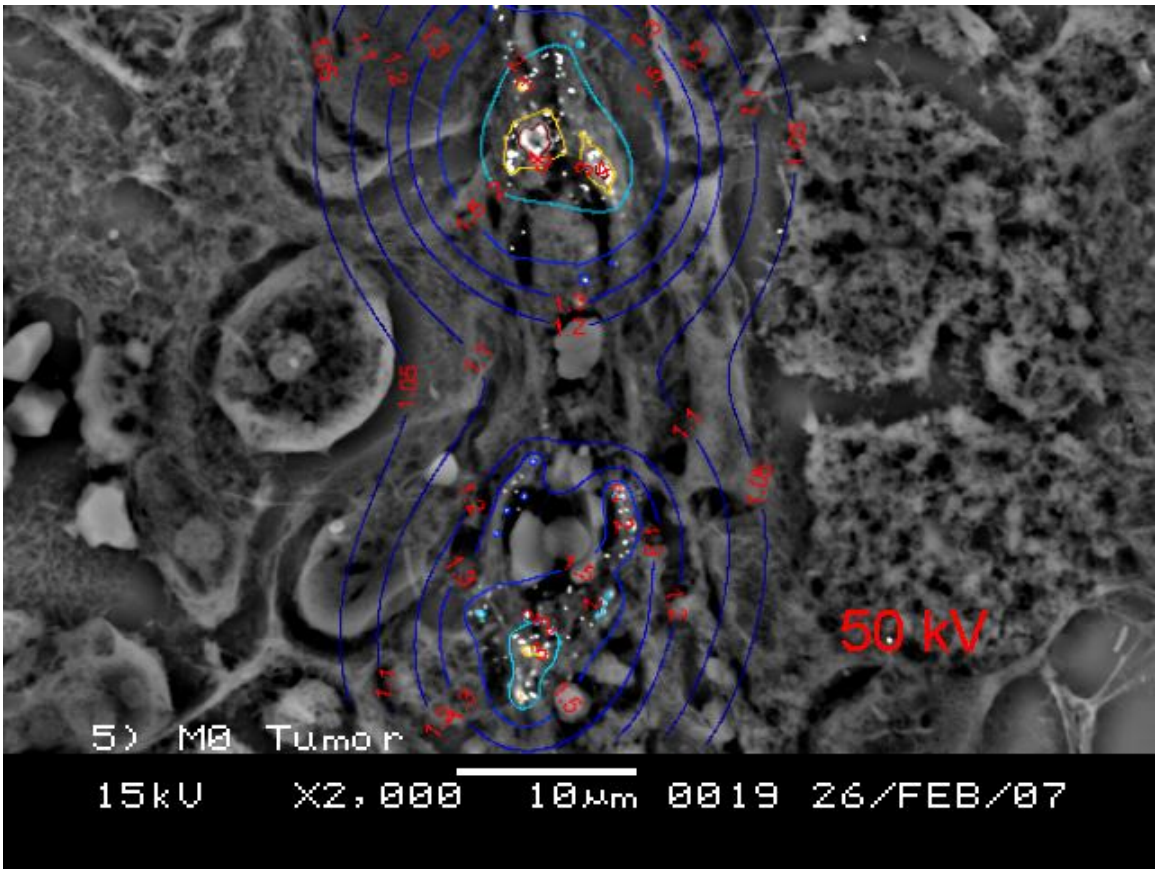

Figure 4.7: Microscopic Dose Enhancement Factor for 50 kVp x-rays

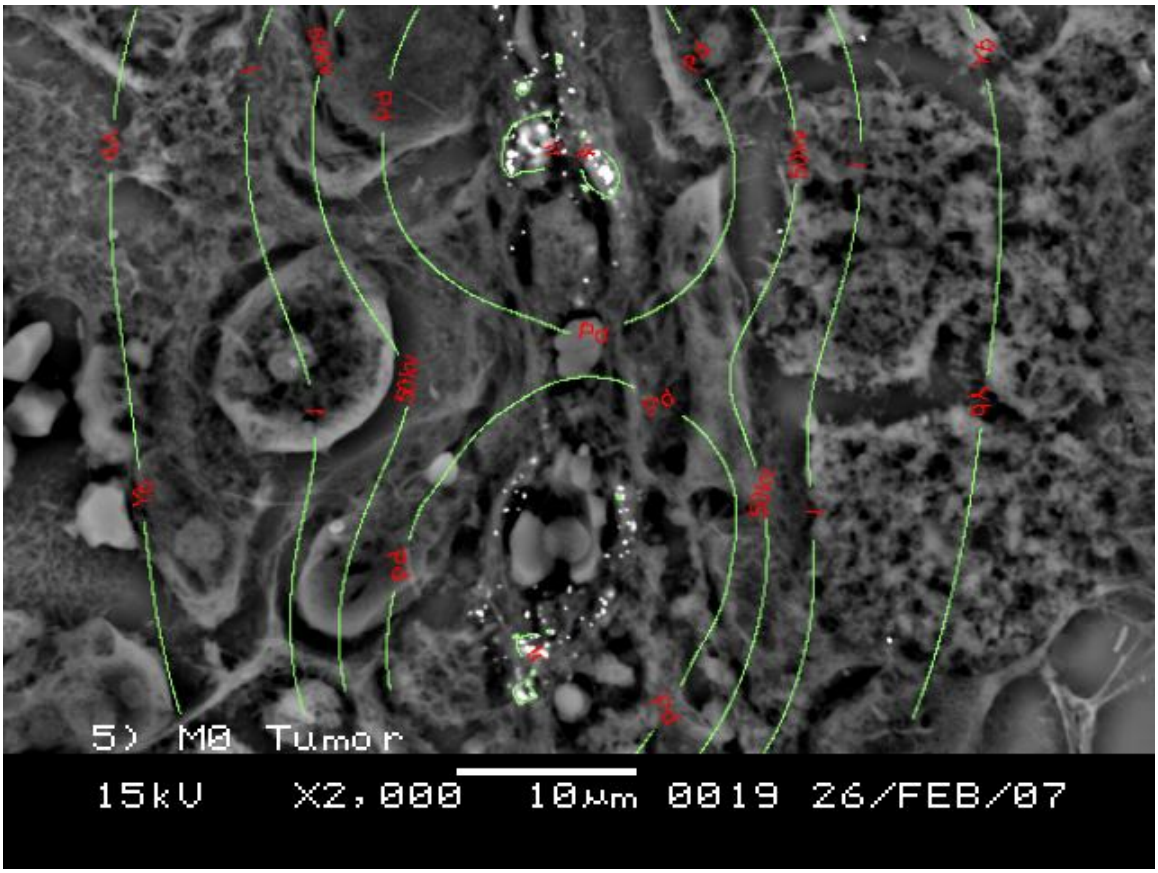

Figure 4.8: Extent of 5% Microscopic Dose Enhancement Line for All Sources

CHAPTER 5

DISCUSSION

The dose point kernels and microscopic dose enhancement factor shed new insight into the results obtained by previous computational studies (Cho 2005, Cho et al 2009). Whereas the macroscopic dose enhancement for ^{125}I, ^{169}Yb, 50 kVp, and ^{192}Ir ranged from 50% to 100% at a gold concentration of 7 mg/g tumor (Cho *et al* 2009), it is seen here that the dose point kernel is enhanced by factors ranging from 10 to 100, and the microscopic dose is enhanced by over 100% over short distances for a gold nanoshell concentration of only 10 μg/g tumor. Moreover, significant variation can be seen between the different source cases. This could allow for the possibility of tailoring the source to the specific biodistribution *in vivo*. For instance, microscopic dose with ^{125}I or 50 kVp can exceed 400% over short distances, allowing for large increases in effectiveness if the gold nanoparticles can be brought within sufficient distance of the targeted cells. On the other hand, irradiation using ^{169}Yb leads to a meaningful dose increase over a larger distance, and could still be effective given a more heterogeneous distribution of nanoparticles.

Given that the dose enhancement exceeds 100% within very short (10 μm) distances from the nanoparticles, it is likely that cell killing could be greatly enhanced by using an active targeting system rather than relying on passive extravasation. Active targeting of nanoparticles to tumors and/or tumor vasculature using peptides, antibodies, and oligonucleotides could not only enhance the tumor loads of gold nanoparticles due to higher nanoparticle specificity, but could also bring the nanoparticles close enough to the

cellular nucleus to dramatically increase the number of deoxyribonucleic acid (DNA) strand breaks. Active targeting would significantly increase the efficiency of the dual mechanisms of action (i.e., direct cell-killing and tumor blood vessel disruption) of gold nanoparticles and x-rays.

CHAPTER 6

FUTURE WORK

There are some considerations which would need to be addressed in future GNRT studies. As the secondary electron dose deposition kernels were calculated in an infinite medium of water, this study ignored self-shielding of the nanoparticles. While it is true that the nanoparticles (1-2 nm) are nearly 100 times smaller than the thickness of the dose collection regions (100 nm), the larger interaction cross section of gold could lead to a change in the dose deposition point kernels. Also, there are other effects such as nanoparticle clumping which could cause the nanoparticles to influence the dose deposition of one another. A more accurate simulation would be one which takes into account the effects that nanoparticles have on themselves and each other rather than considering the nanoparticles on an individual basis.

In addition, the image from which dose was calculated was of gold nanoshells which are unable to effectively penetrate into the tumor interstitium. While these results are certainly promising, it is certainly possible to achieve better microscopic dose enhancement with both a higher gold concentration and smaller particle size. An image taken under these conditions would hopefully better demonstrate the potential of GNRT.

The results of this study could be expanded to create a more accurate biological model of tumor cell killing rather than simply dose enhancement. While it is true that dose corresponds well with cell killing, it would be possible to use the sub-micrometer resolution of the electron point dose kernels to create a model to determine the number of DNA strand breaks, and more directly calculate tumor cell death.

CHAPTER 7

CONCLUSIONS

It has been shown that the infusion of a tumor with 0.7 mg/g gold nanoparticles leads to a dramatic increase in the number and total energy of secondary electrons produced. For low energy photon sources such as ^{169}Yb, ^{125}I, ^{103}Pd, or 50 kVp x-rays, the point dose kernel of secondary electrons is increased by factors ranging from 10 to 100 over 30 μm. For a sample case involving 10 μg Au per gram tumor, this has been shown to cause a meaningful (5%) increase in the microscopic dose to the surrounding cells as far away as 30 μm, and a substantial (100%) increase within 10 μm.

This study demonstrates the potential of obtaining clinically significant dose enhancement with GNRT using commercially available brachytherapy sources. Moreover, the dose enhancement results obtained were for a gold concentration of only 10 μg Au/g tumor, whereas animal studies have found that concentrations as high as 10 mg Au/g tumor can be achieved without significant toxicity (Hainfeld et al 2004). Provided that the biodistribution and toxicity data from animal studies are applicable to humans, these results indicate that it would be feasible to implement GNRT via brachytherapy using ^{169}Yb, ^{125}I, or 50 kVp x-rays. Moreover, due to the differing microscopic energy deposition among these sources, it would be possible to tailor the source and delivery method to achieve the maximum effect for differing treatment types.

APPENDIX A

SECONDARY ELECTRON SPECTRA

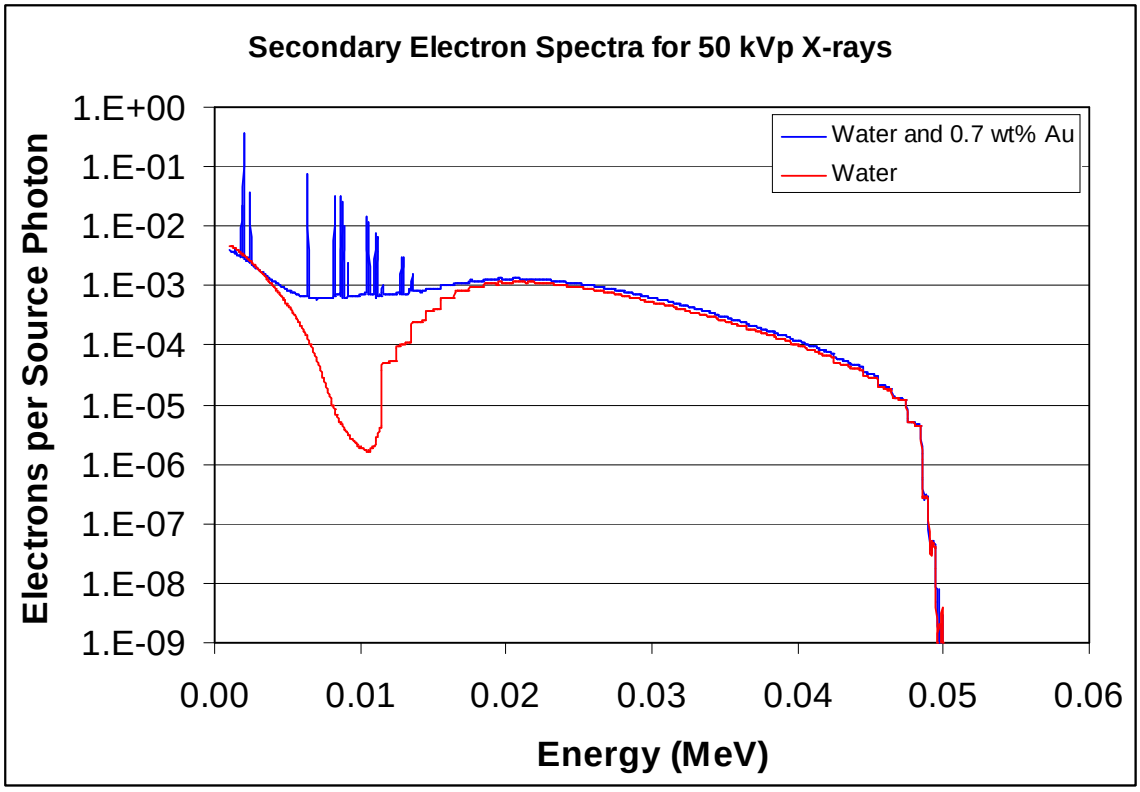

Figure A.1: Secondary Electron Spectra for 50 kVp X-ray Source

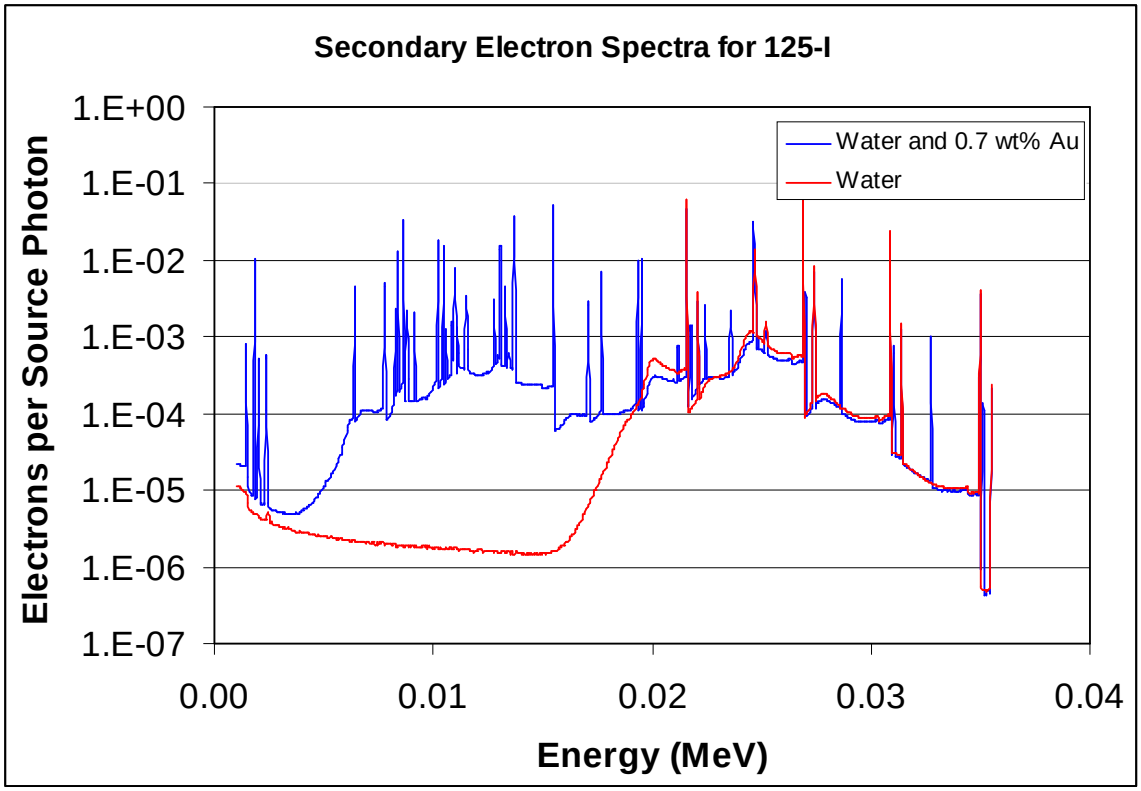

Figure A.2: Secondary Electron Spectra for ^{125}I Source

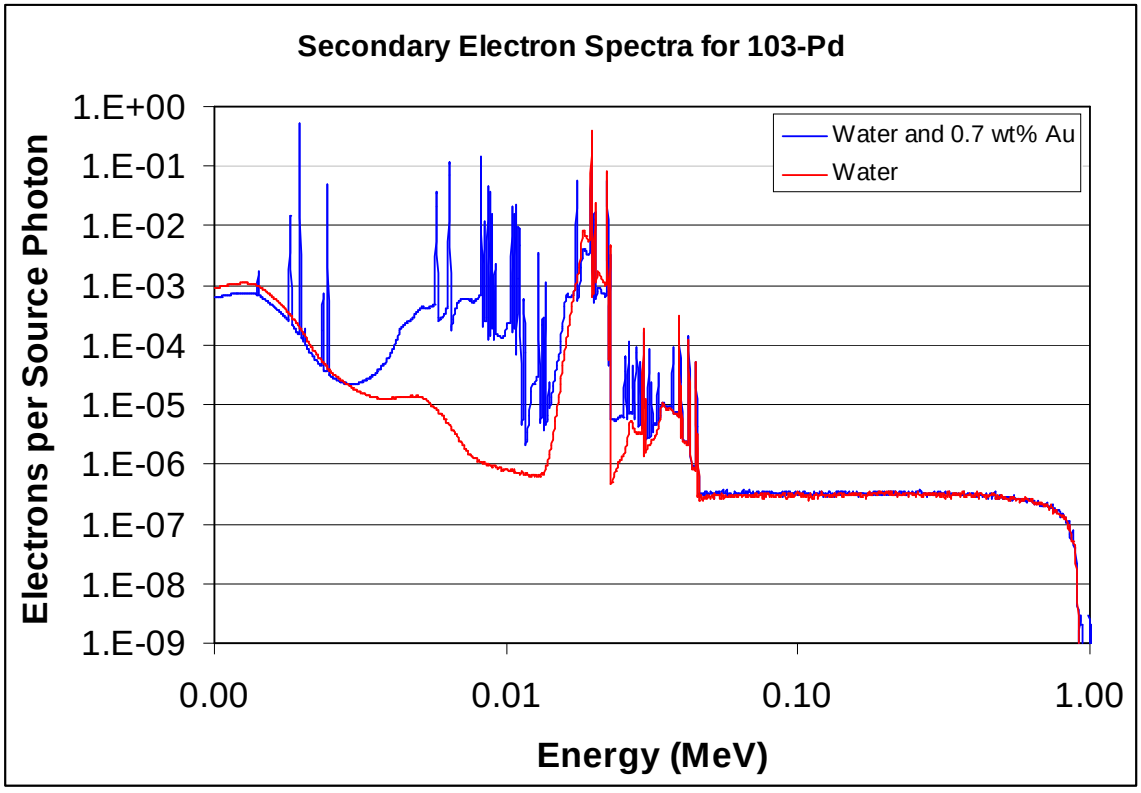

Figure A.3: Secondary Electron Spectra for ^{103}Pd Source

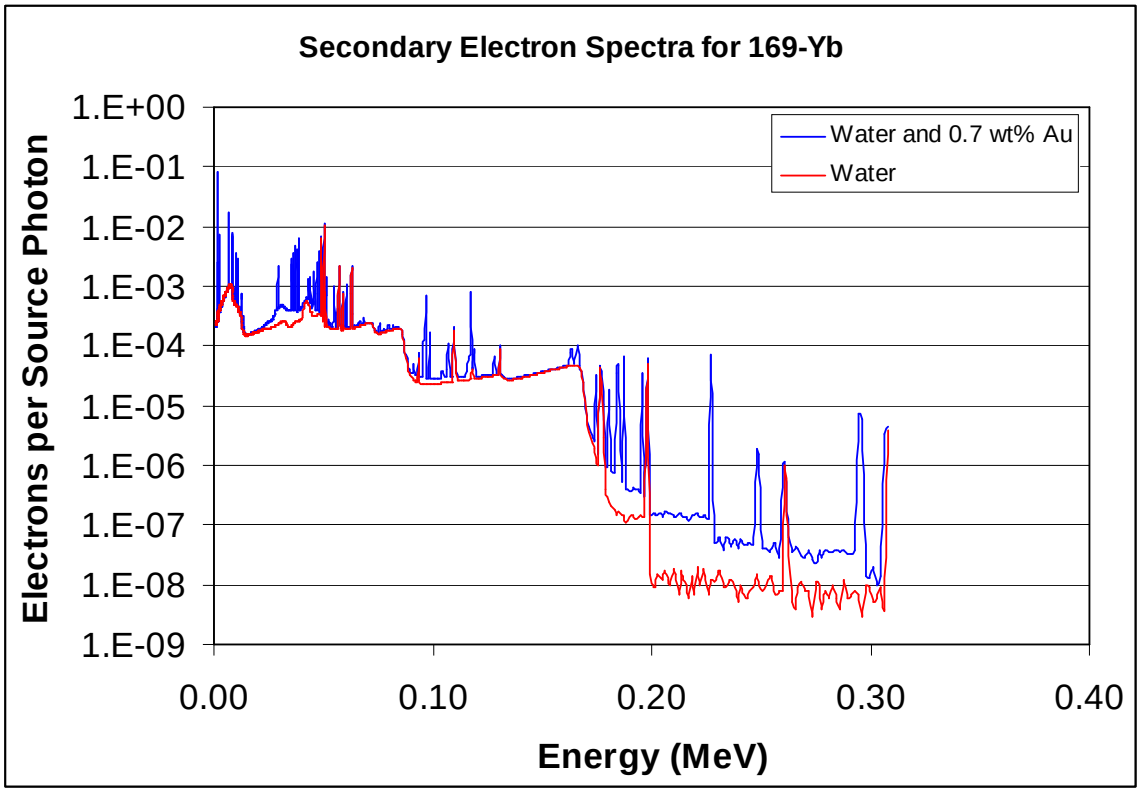

Figure A.4: Secondary Electron Spectra for ^{169}Yb Source

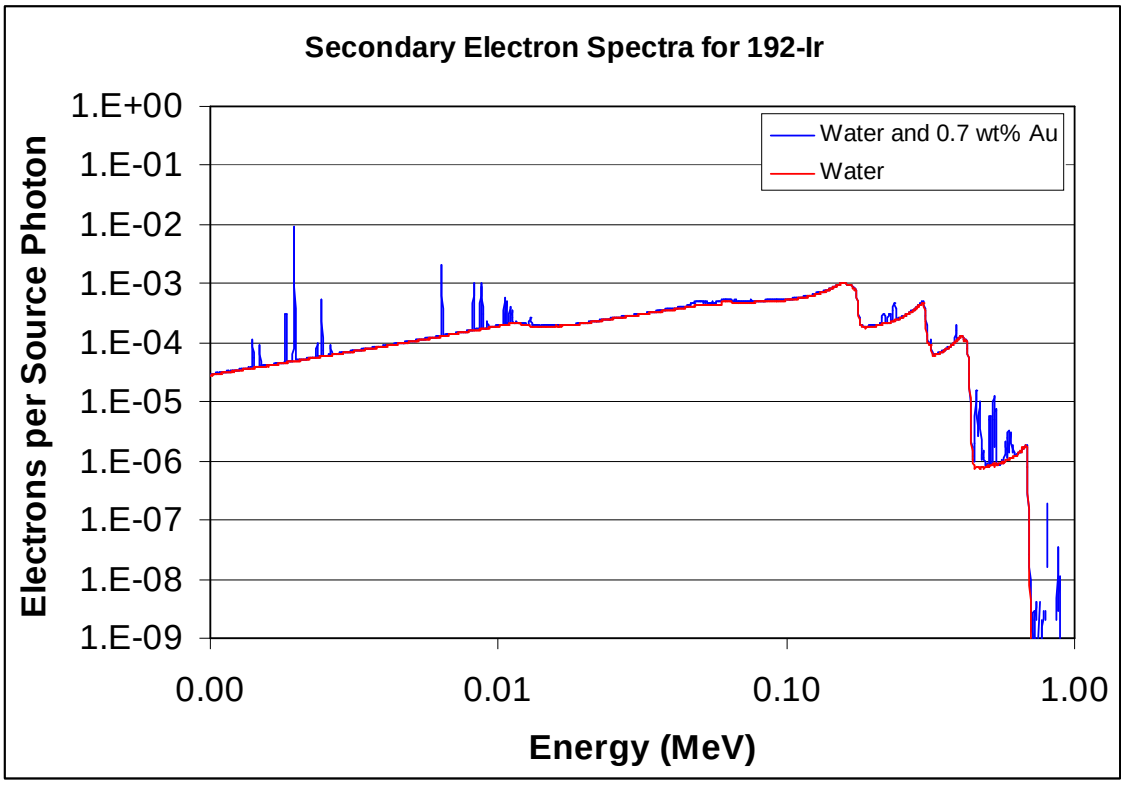

Figure A.5: Secondary Electron Spectra for ^{192}Ir Source

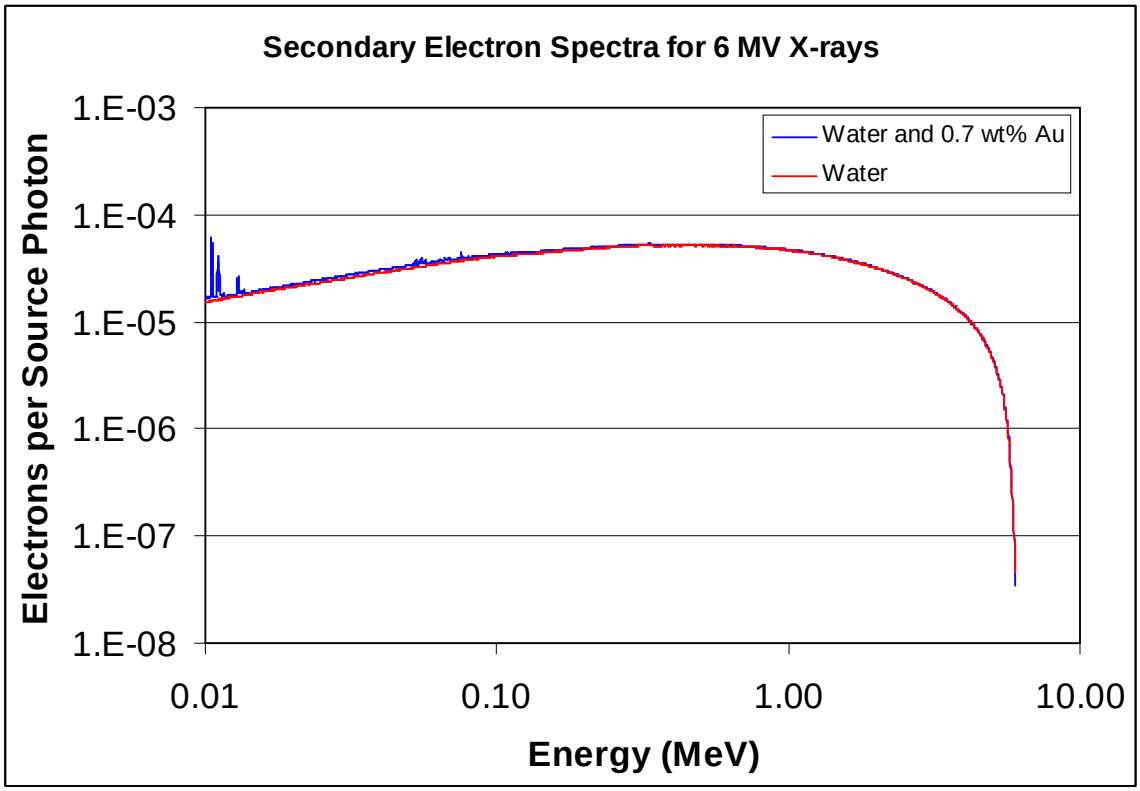

Figure A.6: Secondary Electron Spectra for 6 MV X-ray Source

REFERENCES

Bielajew AF, Hirayama H, Nelson WR, Rogers DWO. 1994 "History, overview, and recent improvements of EGS4," *Report NRCC/PIRS-0436*

Birch R, Marshall M, Ardran GM. 1979 "Catalogue of spectral data for diagnostic x-rays," *Scientific Report **30***

Chen Z and Nath R. 2001 "Dose rate constant and energy spectrum of interstitial brachytherapy sources," *Med. Phys.* **28 (1)** 86-96

Cho SH, Vassiliev ON, Lee S, Liu HH, Ibbott GS, Mohan R. 2005 "Reference photon dosimetry data and reference phase space data for the 6 MV photon beam from Varian Clinac 2100 series linear accelerators" *Med. Phys.* **32 (1)** 137-148

Cho SH. 2005 Estimation of tumor dose enhancement due to gold nanoparticles during typical radiation treatments: A preliminary Monte Carlo study, *Phys. Med. Biol.*, **50(15)** N163-N173

Cho SH, Jones BL, Krishnan S. 2009 Dosimetrtic feasibility of gold nanoparticle-aided radiation therapy (GNRT) via brachytherapy using low energy gamma-/x-ray sources, *Phys. Med. Biol.*, **In Press**

Dawson P, Penhaligon M, Smith E and Saunders J 1987 Iodinated contrast agents as radiosensitizers Br. J. Radiol. 60 201-203

Diagaradjane P, Shetty A, Wang J, Schwartz J, Elliot AM, Shentu S, Park HC, Deorukhkar A, Stafford RJ, Cho SH, Tunnell JW, Hazle JD, Krishnan S. 2008 "Modulation of in vivo tumor radiation response via gold nanoshell mediated vascular-focused hyperthermia: Characterizing an integrated antihypoxic and localized vascular disrupting targeting strategy," *Nano Letters*, **8 (5)** 1492-1500

Dvorak HF, Nagy JA, Dvorak JT, Dvorak AM. 1988 "Identification and characterization of the blood vessels of solid tumors that are leaky to circulating macromolecules," *Am. J. Pathol.* **133** 95-109

Hainfeld JF, Slatkin DN, Smilowitz HM. 2004 "The use of gold nanoparticles to enhance radiotherapy in mice," *Phys. Med. Biol.* **49** N309-N315

Iwamoto K S, Cochran S T, Winter J, Holburt E, Higashida R T and Norman A 1987 Radiation dose enhancement therapy with iodine in rabbit VX-2 brain tumors Radiother Oncol. 8 161-170

Kawrakow I and Rogers DWO. 2003 "The EGSnrc Code System" *National Research Council Report PIRS-701* (Ottawa, Canada)

Ling CC, Yorke ED, Spiro IJ, Kubiatowicz D, Bennett D. 1983 ‘‘Physical dosimetry of 125I seeds of a new design for intersititial implant,’’ *Int. J. Radiat. Oncol., Biol., Phys*. **9**, 1747–1752

Maeda H, Fang J, Inutsuka T, Kitamoto Y. 2003 “Vascular permeability enhancement in solid tumor: various factors, mechanisms involved and its implications,” *International Immunopharmacology*. **3(3)** 319-328

Medich DC, Tries MA, Munro JJ. 2006 “Monte Carlo characterization of an ytterbium-169 high dose rate brachytherapy source with analysis of statistical uncertainty,” *Med. Phys.* **33 (1)** 163-172

Mello R S, Callison H, Winter J, Kagan A R and Norman A 1983 Radiation dose enhancement in tumors with iodine Med. Phys. 10 75-78

Mesa A V, Norman A, Solberg T D, DeMarco J J and Smathers J B 1999 Dose distribution using kilovoltage x-ray and dose enhancement from iodine contrast agents Phys. Med. Biol. 44 1955-1968

Robar J L, Riccio S A and Martin M A 2002 Tumor dose enhancement using modified megavoltage photon beams and contrast media Phys. Med. Biol. 47 2433-2449

Robar J L 2006 Generation and modeling of megavoltage photon beams for contrast-enhanced radiation therapy Phys. Med. Biol. 51 5487-5504

Roeske J C, Nunez L, Hoggarth M, Labay E, Weichselbaum R R 2007 Characterization of the theoretical radiation dose enhancement from nanoparticles Technol. Cancer Res. Treat. 6 395-402

Rose J H, Norman A and Ingram M 1994 First experience with radiation therapy of small brain tumors delivered by a computerized tomography scanner Int. J. Radiat. Oncol. Biol. Phys. 30 24-25

Semenenko VA, Turner JE, Borak TB. 2003 “NOREC, a Monte Carlo code for simulating electron tracks in liquid water,” *Radiation and Environmental Biophysics*. **42 (3)** 213-217

Verhaegen F, Reniers B, Deblois F, Devic S, Seuntjens J, and Hristov D 2005 Dosimetric and microdosimetric study of contrast-enhanced radiotherapy with kilovolt x- rays Phy. Med. Biol. 50 3555-69

Unezaki S, Maruyama K, Hosoda J.-I., Nagae I, Koyanagi Y, Nakata M, Ishida O, Iwatsuru M and Tsuchiya S 1996 Direct measurement of the extravasation of polyethyleneglycol-coated liposomes into solid tumor tissue by in vivo fluorescence microscopy Int. J. Pharm. 144 11-17